European Journal of Medicinal Chemistry 213 (2021) 113171

Contents lists available at ScienceDirect

European Journal of Medicinal Chemistry

journal homepage: http://www.elsevier.com/locate/ejmech

Research paper

Design, synthesis and biological evaluation of novel benzoxaborole derivatives as potent PDE4 inhibitors for topical treatment of atopic dermatitis

Zhaoxing Chu [a, b, c], Qinlong Xu [c, d], Qihua Zhu [a, b], Xiaodong Ma [d], Jiajia Mo [c], Gaofeng Lin [c], Yan Zhao [c], Yuanfeng Gu [c], Lincui Bian [c], Li Shao [c], Jing Guo [c], Wenfeng Ye [c], Jiaming Li [d], Guangwei He [c, **], Yungen Xu [a, b, *]

[a] Department of Medicinal Chemistry, China Pharmaceutical University, Nanjing, 211198, China
[b] Jiangsu Key Laboratory of Drug Design and Optimization, China Pharmaceutical University, Nanjing, 21009, China
[c] Hefei Institute of Pharmaceutical Industry Co., Ltd., Hefei, 230088, China
[d] Department of Medicinal Chemistry, Anhui University of Chinese Medicine, Hefei, 230031, China

ARTICLE INFO

Article history:
Received 23 November 2020
Received in revised form
7 January 2021
Accepted 7 January 2021
Available online 12 January 2021

Keywords:
Benzoxaborole derivatives
Atopic dermatitis
Isoform specificity
In vivo efficacy
Safety

ABSTRACT

In this work, a series of structurally novel benzoxaborole derivatives were designed, synthesized and biologically evaluated as PDE4 inhibitors for battling atopic dermatitis (AD). Among them, the majority exhibited superior PDE4B inhibitory activities to that of the lead compound Crisaborole, an approved PDE4 inhibitor. In particular, **72**, the most potent PDE4B inhibitor throughout this series, displayed 136-fold improved enzymatic activity (IC_{50} = 0.42 nM) as compared to Crisaborole (IC_{50} = 57.20 nM), along with favorable isoform specificity. In the phorbol ester (PMA)-induced mouse ear oedema model, **72** exerted remarkably greater efficacy than Crisaborole at the same dosage ($P < 0.05$). Moreover, the ointment of **72** exerted dramatically enhanced therapeutic potency than the ointment of Crisaborole ($P < 0.05$) in the calcipotriol-induced mouse AD model. In addition to the potent *in vitro* and *in vivo* activity, **72** displayed favorable safety in the repeated oral dose toxicity study and did not exhibit phototoxicity. With the above attractive biological performance, **72** is worthy of further functional investigation as a novel anti-AD therapeutic agent.

1. Introduction

Atopic dermatitis (AD) is the most common chronic inflammatory skin disorder affecting young children. The prevalence of AD is continuously increasing, with approximately 20% of children and 1%–3% of adults suffering from it in developed countries [1]. Depending on the duration of the lesions, individuals bearing AD experience pruritus, erythema, and dermatitic plaques which may weep, crust or scale [2,3]. Currently, topical corticosteroids are frequently prescribed for battling AD in clinic. However, the toxicity resulted from the long-term treatment hindered their extensive application. Hence, the development of nonsteroidal tropical anti-inflammatory agents for combating AD is in urgent demand [4,5].

Massive efforts have been undertaken by the research community to unravel the exact etiology of AD. Although it remains ambiguous, numerous studies have implicated the epidermal barrier defects and the dysregulation of the immune system in the pathogenesis of AD [6,7]. Cyclic adenosine monophosphate (cAMP)-related signaling cascades play a critical role in regulating the immune function. Under normal physiological conditions, the cellular level of cAMP is retained by a dynamic equilibrium between the biosynthesis and cyclic nucleotide phosphodiesterases (PDEs)-catalyzed decomposition [8]. The involvement of PDE4, the most diverse family of PDEs, in a broad spectrum of inflammatory disorders renders it a promising therapeutic target for these diseases. Upon the inhibition of PDE4, the elevated intracellular cAMP level triggers specific protein phosphorylation cascades and consequently induces a variety of functional responses in the inflammatory cells, exemplified by the downregulation of tumor necrosis factor alpha (TNF-α) production [9–11].

* Corresponding author. Department of Medicinal Chemistry, China Pharmaceutical University, Nanjing, 211198, China.
** Corresponding author.
E-mail addresses: heguangwei@ahipi.com (G. He), xyg@cpu.edu.cn (Y. Xu).

https://doi.org/10.1016/j.ejmech.2021.113171
0223-5234/

The four subtypes of PDE4, termed as PDE4A, B, C and D, are predominantly expressed in inflammatory and immune cells, including B cells, T cells and macrophages. In particular, PDE4B and PDE4D participate in modulating the liberation of pro-inflammatory mediators and regulating neutrophil function, thereby attracting considerable attention in both academic area and pharmaceutical industry as anti-inflammatory targets. So far, Roflumilast **(1)**, Apremilast **(2)**, Cilomilast **(3)** and Crisaborole **(4)**, as PDE4 inhibitors, have been approved for treating inflammation-related diseases (Fig. 1). While **1**–**3** are applied to treat asthma and arthritis upon oral administration, **4** is a nonsteroidal topical anti-AD agent, which is capable of suppressing the release of inflammatory cytokines, including TNF-α, IL-2, IL-5 and interferon-γ (IFN-γ) [12]. However, approximately 25% patients fail to benefit from **4** and need rescue therapy with either topical corticosteroids or topical tacrolimus [13,14]. Additionally, some patients receiving Crisaborole treatment suffer from local skin irritation.

For surmounting the aforementioned drawbacks, we have recently initiated a medicinal chemistry campaign to discover effective and more specific PDE4 inhibitors. Our insight into the crystal structure of AN2898 (5, Fig. 1), a Crisaborole derivative, complexed with PDE4B catalytic site provided a foundation for the rational design of novel PDE4 inhibitors from **4**. AN2898 assumed a distinct binding mode from other PDE4 inhibitors with the boron atom coordinated to the water molecule held and activated by zinc and magnesium ions (Fig. 2A and B). Provided this, the boron adopted a tetrahedral form and mimicked the phosphate group of AMP, hence conferring similar interactions with the metal ions [15]. These interactions were necessary for PDE4 binding affinity. Nonetheless, the substituted phenyl of AN2898 was merely located at the entrance to the adenine pocket formed by side chains of residues Phe 446, Ile 410 and Gln 443 (Fig. 2C). Therefore, further interactions with residues in this pocket may be beneficial to enhancing the potency and specificity. Based on this consideration, a structure-based drug design approach was employed in this work via replacing the substituted phenyl of Crisaborole with structurally diverse bicyclic fragments for exploiting the adenine pocket (Fig. 3). Besides, as revealed by the reported SARs and pharmacophore feature of the benzoxaborole-drived PDE4B inhibitors, electron-withdrawing groups and H-bond acceptors on the substituents tethered to the oxygen at C-5 position of the benzoxaborole core were beneficial to the enzymatic activity. Hence, we prioritized introduction of bicyclic scaffolds bearing electron-withdrawing substituents or H-bond acceptors to replace the cyanophenyl. Upon the strategy stated above, a novel series of Crisaborole analogues were designed, synthesized, and biologically evaluated, which led to the discovery of **72**, a highly potent and selective PDE4B inhibitor with excellent performance both *in vitro* and *in vivo*. In addition to the remarkable efficacy, **72** featured favorable safety profile. Owing to these advantages, it has the potential to be an anti-AD candidate for further development.

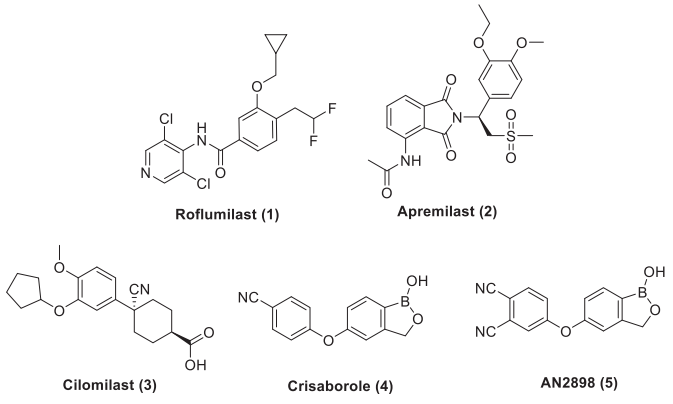

Fig. 1. The chemical structures of the four approved PDE4 inhibitors and Crisaborole derivative AN2895.

2. Results and discussion

2.1. Chemistry

Scheme 1 described the synthetic route to compounds **29**–**32** [16–21]. 1-(2,4-Dihydroxyphenyl) ethan-1-one **6**, as the starting material, was condensed with triethyl orthoformate to afford 7-hydroxy-4*H*-chromen-4-one **7** [22]. 7-Hydroxy-2,2-dimethylchroman-4-one **10** was prepared via condensation of resorcinol with 3,3-dimethacrylic acid and subsequent intramolecular cyclization in the presence of NaOH. Subsequently, **7** and **10**–**12** were subjected to SNAr reaction with 5-fluoro-2-nitrobenzaldehyde in the presence of K_2CO_3 to provide **13**–**16.** Reduction of the nitro functionality of **13**–**16** and the following Sandmeyer reaction led to the generation of **21**–**24** as the intermediates. Afterwards, they were converted into corresponding boric acid esters **25**–**28**, which further underwent one-pot reduction of the aldehyde moiety and the intramolecular cyclization, as well as the hydrolysis after treatment with 6 N HCl to furnish target compounds **29**–**32** [23,24].

Scheme 2 depicted the preparative method for compounds **63**–**72**. SNAr reaction of the imidazopyrimidine derivative **33** or the quinoline derivatives **34**–**42** with 2-bromo-5- hydroxybenzaldehyde in the presence of K_2CO_3 provided **43** and **44**–**52**, respectively. They were then transformed into corresponding boric acid esters, which experienced a similar route to Scheme 1 to afford **63** and **64**–**72** as the target compounds [25–27]. The structures of all the compounds were characterized by ^{13}C NMR, ^{1}H NMR and HRMS.

2.2. PDE4B inhibitory activity

All the target compounds were evaluated for their PDE4B inhibitory activities with Crisaborole as the positive reference. The results demonstrated that a majority of them exhibited superior PDE4B inhibitory activities to that of Crisaborole, thereby validating the rationality of the compound design. In particular, six compounds, that are **64, 65, and 69**–**72**, displayed single-digit nanomolar or subnanomolar IC_{50} values. Compound **72** was the most active PDE4B inhibitor throughout this series with IC_{50} value of 0.42 nM, which was 136-fold more potent than Crisaborole. From the enzymatic activity shown in Table 1, some valuable structure-activity relationships (SARs) can be concluded. In general, quinoline as the bicyclic substituent was beneficial to PDE4B inhibitory activity, which can be revealed by the more potent activities of **64**–**67** and **69**–**72** than those of **29**–**32**. According to the biological data of **64**–**66**, it became evident that the position of COOMe at the quinoline moiety did not significantly affect the potency. However, replacement of the COOMe (**64**) at the C-5 position of the quinoline with COOEt (**67**) and COOH (**68**) led to a decrease in PDE4B inhibitory activity. Particularly, the introduction of polar COOH weakened the activity to submicromolar level. When COOH was replaced by non-polar $COCH_3$ and CF_3 groups, the decrease in activity was reversed, and both the resultant compounds **69** and **70** exhibited single-digit nanomolar IC_{50}s. Hence, polar substituents at the quinoline had a detrimental effect on potency. To our delight, when CF_3 substituted the C-6 position of the quinoline, **72**, the most potent compound throughout this series, was attained.

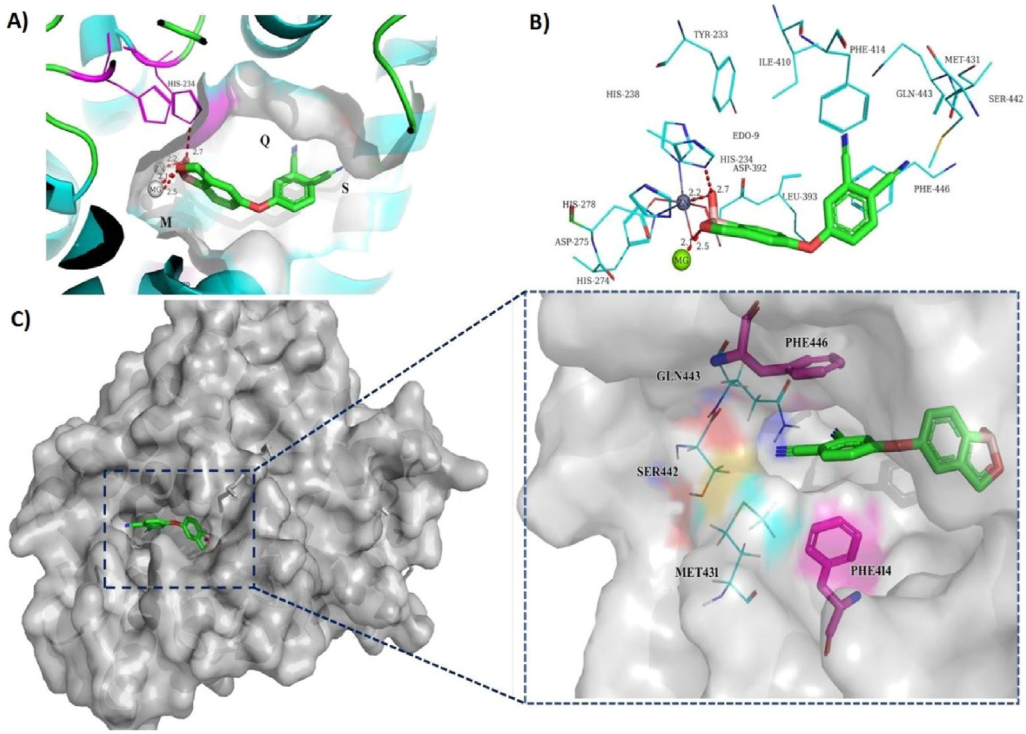

Fig. 2. Co-crystal structure of AN2898 with the active site of PDE4B catalytic domain [15].

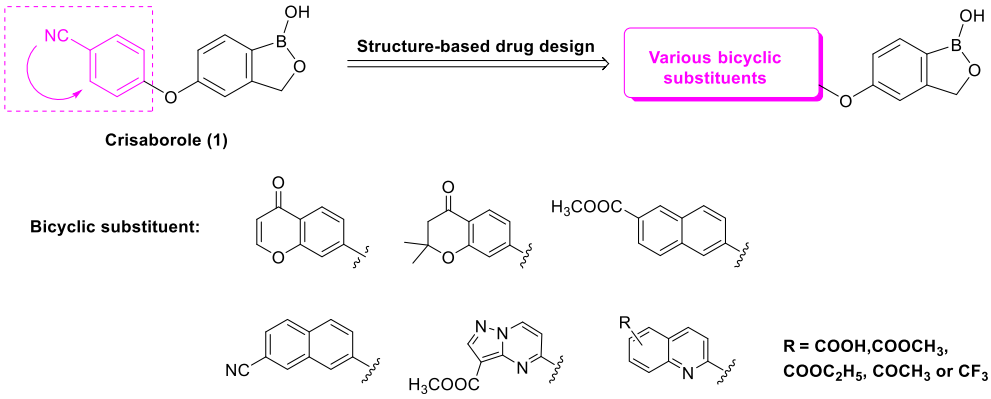

Fig. 3. The design rationale of target Crisaborole derivatives.

2.3. Effect on phorbol myristate acetate (PMA)-induced mouse ear oedema

Based on the PDE4B inhibitory activity, nine compounds were chosen for evaluating their anti-inflammatory activities against the PMA-induced mouse ear oedema [28,29], and the results were shown in Table 2. Compared with the blank, the model group showed a dramatically increased swelling degree ($P < 0.01$), indicating the availability of the model. The results illustrated that the swelling degree was obviously reduced ($P < 0.05$, $P < 0.01$) by a majority of compounds except **65** and **71** after 1 mg/ear. Among the effective compounds, compound **72** induced the most remarkable decrease in swelling degree with the inhibition rate of 65.85%, and its efficacy surpassed that of Crisaborole at the same dosage. The distinguished efficacy of **72** was consistent with its high PDE4B inhibitory activity.

2.4. Isoform specificity

Compound **72**, as the representative of this series, was then evaluated for its specificity over other PDE isoforms. In general, the specificity of **72** for PDE4B was more favorable over that of Crisaborole, according to experimental results shown in Table 3. In particular, it exhibited over 10,000-fold selectivity over PDE3A, PDE3B and PDE10A, and the specificity over these isoforms was much higher than that of Crisaborole.

2.5. Effect on calcipotriol-induced AD in mice

By virtue of its attractive performance stated above, **72** was formulated as ointment and further evaluated for its efficacy against calcipotriol-induced mouse AD model [30,31]. As revealed by the data presented in Table 4, treatment with the ointment of **72**

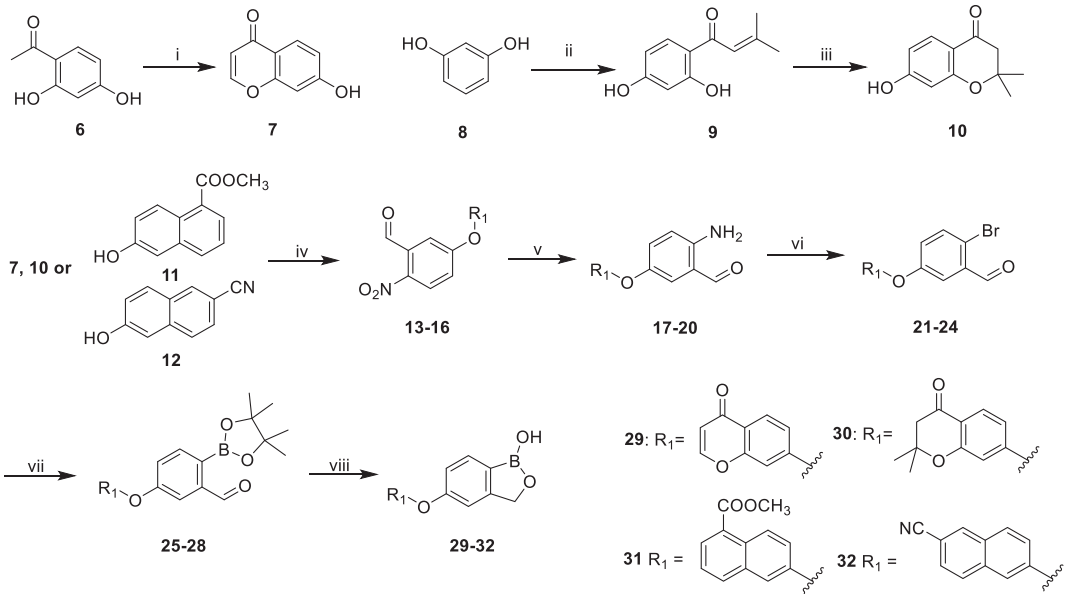

Scheme 1. Reagents and conditions: (i) 70% $HClO_4$, Triethyl orthoformate, rt., 10min; (ii) 3,3-dimethacrylic acid, $ZnCl_2$, $POCl_3$, rt., 2 h; (iii) 5% NaOH, rt., 1 h; (iv) 5-fluoro-2-nitrobenzaldehyde, K_2CO_3, DMF, rt., 24 h; (v) Fe, NH_4Cl, EtOH/H_2O, 80 °C, 2.5 h; (vi) CuBr, t-BuONO, CH_3CN, −10 °C, 0.5 h; (vii) B_2pin_2, Pd (dppf)Cl_2, AcOK, 1, 4-dioxane, 90 °C, 1.5 h; (viii) $NaBH_4$, 6 N HCl, CH_3OH, 0 °C,1 h.

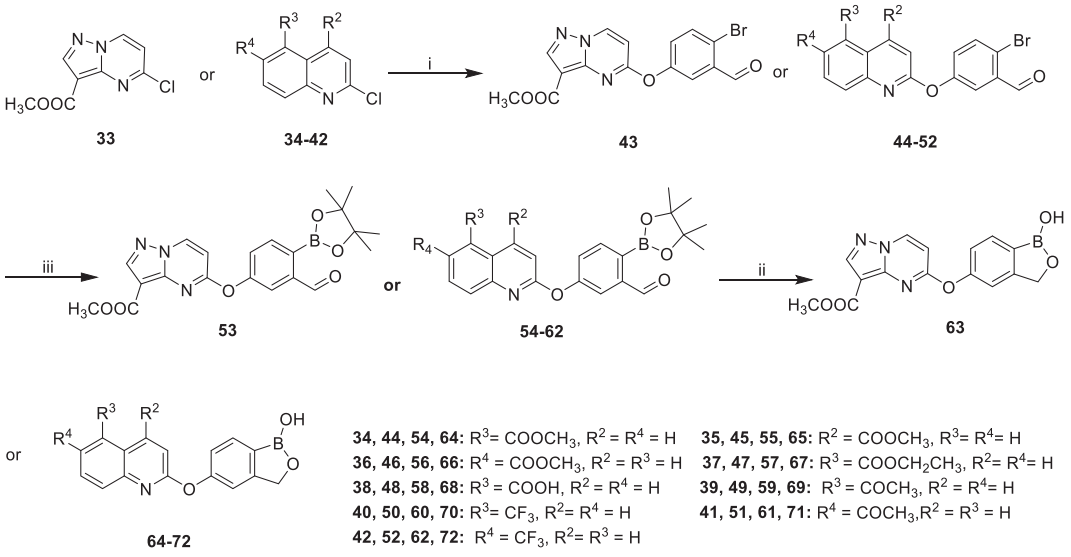

Scheme 2. Reagents and conditions: (i) 2-bromo-5-hydroxybenzaldehyde, K_2CO_3, DMF, 100 °C, rt., 24 h; (ii) B_2pin_2, pd (dppf)Cl_2, AcOK, 1, 4-dioxane, 100 °C, 2 h; (vi) $NaBH_4$, HCl, CH_3OH, rt., 0.5 h.

caused obvious decrease in swelling degree at the dose of 30 mg/ear. Importantly, the ointment with 2% **72** resulted in more remarkable efficacy than ointment with 2% Crisaborole at the same dosage, and the inhibition rate was 73.33%.

2.6. Repeated dose toxicity

We further performed a preliminary repeated oral dose toxicity study of **72** in order to evaluate its safety profile. The 14-consecutive-day oral administration of compound **72** did not cause any systemic toxicity or animal death even at a dose as high as 700 mg/kg. No significant difference was observed in the liver/brain index, kidney/brain index, spleen/brain index and white blood cell count, ALT, AST, blood pressure, and blood glucose, when comparing the 400 mg/kg and 700 mg/kg dose groups with the normal control group in autopsy at the end of the experiment. These results indicated that compound **72** exhibited favorable safety with a no observed adverse effect level (NOAEL) dose over 400 mg/kg.

2.7. Phototoxicity

In addition to the repeated oral dose toxicity, we also evaluated the toxicity of the ointment of **72** induced by UVA irradiation via Lovelland Sander method [32]. As displayed in Table 5, the erythema and oedema occurred in the 8-methoxypsoralen (8-MOP) group at 24 h post-irradiation, and the phototoxicity was diminished from 48 h to 72 h post-treatment. Neither erythema nor

Table 1
PDE4B inhibitory activity of target compounds bearing different various bicyclic.

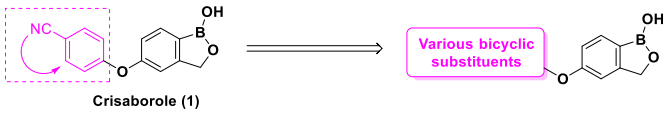

Cpd.	Bicyclic substituents	PDE4B(IC_{50}, nM)	Cpd.	Bicyclic substituents	PDE4B(IC_{50}, nM)
Crisaborole	/	57.20	**66**	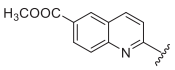	10.79
29	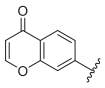	18.90	**67**	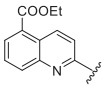	17.29
30	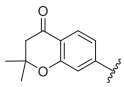	65.50	**68**	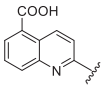	124.1
31	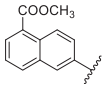	21.88	**69**	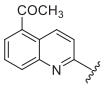	3.05
32	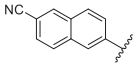	25.49	**70**	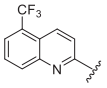	6.42
63	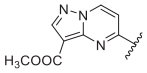	46.20	**71**	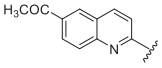	3.57
64	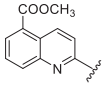	6.44	**72**	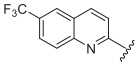	0.42
65	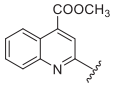	8.25			

Table 2
Effect of selected compounds on PMA-induced oedema in the mouse ear (Mean ± SD, n = 8).

Group	Dose (mg/ear)	Swelling (mm)	Inhibition (%)
blank	/	0.25 ± 0.04	/
model	/	22.55 ± 8.39△△	/
Crisaborole	1.0	12.73 ± 4.75*	43.55
64	1.0	9.53 ± 3.32**	55.62
65	1.0	15.65 ± 5.50	30.60
66	1.0	10.21 ± 4.91**	54.72
67	1.0	9.54 ± 3.49**	57.69
68	1.0	12.85 ± 6.27*	45.76
69	1.0	13.63 ± 3.12*	39.56
70	1.0	9.46 ± 3.99**	58.05
71	1.0	14.88 ± 3.80*	34.09
72	1.0	7.70 ± 2.95**#	65.85

#P < 0.05 statistical significance compared with Crisaborole; *$P < 0.05$.
**$P < 0.01$ compared with model.
△△P < 0.05 compared with blank.

Table 3
Selectivity of compound 72 and Crisaborole over other nine PDE isoforms enzymes.

PDEs	IC_{50}(nM)	
	Crisaborole	72
PDE1A	5600 (85-fold)[a]	64.7 (154-fold)[a]
PDE1B	17,900 (271-fold)[a]	58.0 (138-fold)[a]
PDE1C	71,000 (1076-fold)[a]	866.0 (2062-fold)[a]
PDE2A	3630 (55-fold)[a]	120.0 (286-fold)[a]
PDE3A	64,000 (970-fold)[a]	8130 (19,357-fold)[a]
PDE3B	58,800 (891-fold)[a]	7190 (17,119-fold)[a]
PDE4B	70.0	0.42
PDE5A	56,100 (850-fold)[a]	819 (1950-fold)[a]
PDE7A	2030 (31-fold)[a]	34.7 (83-fold)[a]
PDE10A	97,600 (1479-fold)[a]	4520 (10,762-fold)[a]

a) Selectivity fold.

oedema was monitored in the groups treated by the ointment of **72**, even at a high dose, indicating no phototoxicity of **72.**

We then conducted the pathological analysis, and the results illustrated that the epidermis of Crisaborole-treated (Fig. 4C) and **72-**treated (Fig. 4D–F) groups were intact. Besides, no infiltration of inflammatory cells and necrosis were observed in Crisaborole or **72**-treated (Fig. 4D–F) groups. By contrast, in the 8-MOP group, inflammatory cell infiltration in the dermis and necrotic changes in the epidermis were observed at 72 h in back skin (Fig. 4B). Thus, the treatment with the ointment of **72** did not induce phototoxicity.

2.8. Molecular modeling

To elucidate its possible binding mode with PDE4B, compound **72** was docked into the active site of PDE4B on the basis of the available PDE4B/AN-2898 co-crystal structure (PDB code 3O0J) [33]. As demonstrated in Fig. 5, **72** (blue) assumed a similar binding mode to that of AN-2898 (yelow) (Fig. 5B). The benzoxaborole was

Table 4
The swelling inhibition of selected compounds against calcipotriol-induced mouse AD model (Mean ± SD, n = 10).

Group	Dose (mg/ear)	Thickness (mm)		Swelling	Inhibition (%)
		left ear	right ear		
normal	–	0.26 ± 0.02	0.26 ± 0.02	–	–
model	–	0.26 ± 0.01	0.55 ± 0.06	0.29 ± 0.05	–
2% Crisaborole	30	0.29 ± 0.03	0.37 ± 0.05	0.08 ± 0.04*	32.50
2% **72**	30	0.29 ± 0.03	0.32 ± 0.02	0.03 ± 0.01**▲▲	73.33

*$P < 0.05$.
**$P < 0.01$vs model.
▲$P < 0.05$.
▲▲$P < 0.01$ vs Crisaborole.

Table 5
Skin reaction scores at each time point.

Group	Dose (mg/kg)	Skin reaction score after UVA irradiation			
		1 h	24 h	48 h	72 h
normal	–	0	0	0	0
8-MOP	–	0	3.8 ± 0.8	3.7 ± 0.5	2.5 ± 0.5
72	5	0	0	0	0
	10	0	0	0	0
	24	0	0	0	0
Crisaborole	10	0	0	0	0

engaged in coordination to Mg^{2+} and Zn^{2+} ions, H-bond interaction with His 234, as well as hydrophobic contact with Met 347. Importantly, the quinoline substituent occupied the entrance of a deep hydrophobic pocket and conferred π-π stacking with the aromatic ring of Phe 414 and Phe 285, which may account for the increase in enzymatic potency after the introduction of quinoline as the bicyclic substituent.

3. Conclusions

Given the medicinal potential of PDE4 as anti-AD target, the exploration of PDE4 inhibitors with favorable isoform specificity, therapeutic efficacy and safety will offer benefits for AD patients. In this study, we discovered a series of structurally novel benzoxaborole derivatives as PDE4 inhibitors via structure-based drug design on the basis of Crisaborole, an approved anti-AD agent. A majority of them exerted PDE4B inhibitory activities superior to that of Crisaborole. **72**, the most active compound throughout this series, also exhibited attractive PDE4 specificity, which was 136-fold more potent than Crisaborole. In both PMA-induced mouse ear oedema model and calcipotriol-induced mouse AD model, **72** led to more remarkable therapeutic efficacy than Crisaborole at the same dosage. Moreover, as revealed by the repeated oral dose toxicity study and the phototoxicity investigation, **72** also displayed favorable safety profile. Attributed to its aforementioned excellent *in vitro* and *in vivo* biological performance, it has been progressed into further pre-clinical investigation.

4. Experimental section

4.1. Chemistry

The reagents and solvents for reaction were commercially available, and when necessary, pre-treatment was carried out prior to use. Tetramethylsilane (TMS) was used as the internal standard

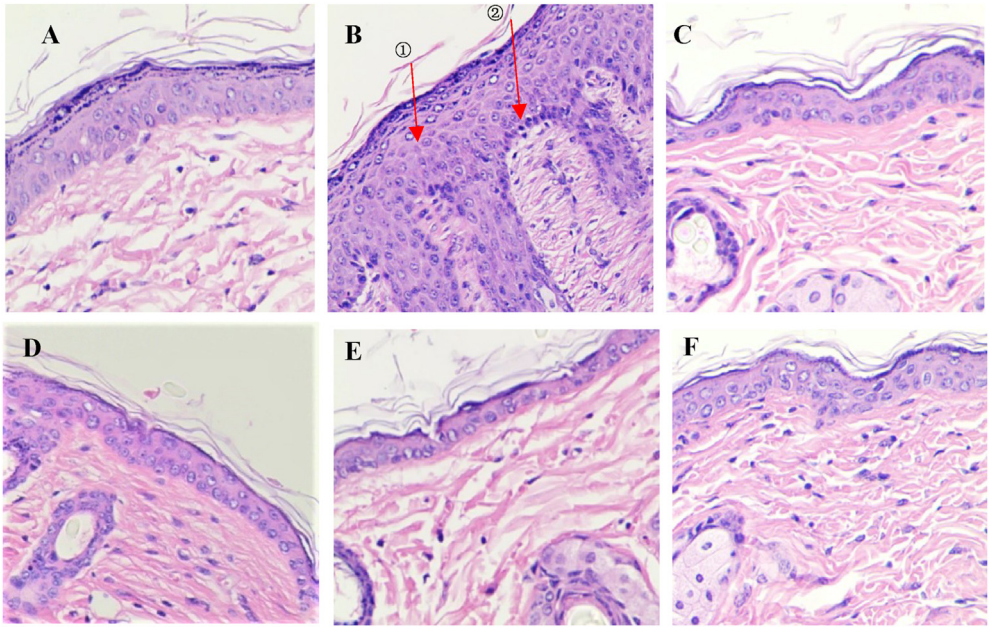

Fig. 4. Representative histopathological findings at 72 h after light exposure in each group (hematoxylin and eosin, scale bar: 50 μm). In the 8-MOP group(B), epidermal thicken (arrow head NO.1) and dermal inflammatory cell infiltration (arrow head NO.2) were observed in the back skin. There were no infiltration of inflammatory cells and necrosis observed in normal (unirradiated) albino guinea pig's skin (A), crisaborole group (C) and 5 mg/kg (D), 10 mg/kg (E), 24 mg/kg (F) of **72** group.

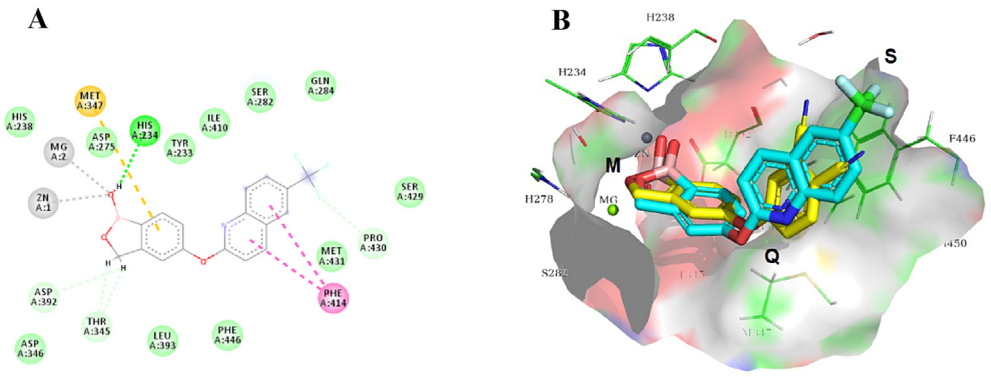

Fig. 5. The molecular docking result of **72** into PDE4B catalytic site (π-π stacking, H-bond contact, and the interaction with metal ion were shown as pink, green and gray dashed line, respectively).

for recording ^{1}H NMR and ^{13}C NMR spectra, and the spectra were obtained with a 400 MHz instrument (Bruker, Fallanden, Switzerland). MS spectra were collected with a Hewlett-Packard 1100 LC/MSD spectrometer (Agilent, Waldbronn, Germany).

4.1.1. 7-Hydroxy-4H-chromen-4-one (7)

To a solution of 1-(2,4-dihydroxyphenyl)ethan-1-one (12.0 g, 0.08 mmol, 1eq) in triethyl orthoformate (30 mL) was added 70% $HClO_4$ (8.4 mL, 0.147 mol, 1.83eq) dropwise within 10 min at room temperature. After being stirred for 3 h, the reaction mixture was treated with anhydrous diethyl ether (216 mL) and the resultant mixture was stirred for 10 min. The mixture was filtered and the filter cake was washed with anhydrous diethyl ether (50 mL × 3). The filter cake was added to boiling water (360 mL) in portions. The mixture was stirred till the water cooled to room temperature. Following filtration, the precipitate was washed with water (100 mL × 3) to afford intermediate **7** as a brown solid. Yield 58.9%; ^{1}H NMR (400 MHz, DMSO-d_6): δ 10.77 (s, 1H), 8.14 (d, J = 6.0 Hz, 1H), 7.88 (d, J = 8.8 Hz, 1H), 6.90–6.93(dd, J_1 = 2.0 Hz, J_2 = 8.8 Hz, 1H), 6.85 (d, J = 2.0 Hz, 1H), 6.21 (d, J = 6.0 Hz, 1H).

4.1.2. 11-(2,4-Dihydroxyphenyl)-3-methylbut-2-en-1-one (9)

To a round bottom flask were added resorcinol (11 g, 0.1 mol, 1eq), 3-methylbut-2-enoic acid (10 g, 0.1 mol, 1eq), $ZnCl_2$ (20.4 g, 0.15 mmol, 1.5eq) and $POCl_3$ (82 mL). After being stirred for 2 h at room temperature, the reaction mixture was cooled to room temperature and poured to ice water (2 L). Following filtration, the precipitate was washed with water (100 mL × 3), and then recrystallized with EtOH/H_2O to give the title intermediate as a white solid. Yield 52.0%; ^{1}H NMR (400 MHz, DMSO-d_6): δ ppm 13.27 (s, 1 H), 10.59 (s, 1 H), 7.83 (d, J = 4.8 Hz, 1 H), 6.91 (m, 1 H), 6.34 (d, J = 8.8 Hz, 1 H), 6.25–6.26 (m, 1 H), 2.14 (d, J = 1.2 Hz, 1 H), 2.01 (d, J = 1.2 Hz, 1 H).

4.1.3. 7-Hydroxy-2,2-dimethylchroman-4-one (10)

To a round bottom flask were added 1-(2,4-dihydroxyphenyl)-3-methylbut-2-en-1-one (10 g, 0.052 mol, 1eq) and 5% NaOH solution (30 mL). After stirring the reaction mixture for 1 h at room temperature, the pH of the mixture was adjusted to 3 with HCl solution (3 N), and precipitation occurred. Following filtration, the precipitate was washed with water (100 mL × 3) to afford the title intermediate as a white solid. Yield 99%; ^{1}H NMR (400 MHz, DMSO-d_6): δ ppm 10.48 (s, 1 H), 7.58 (d, J = 4.2 Hz, 1 H), 6.43 (dd, J_1 = 2.0 Hz, J_2 = 4.2 Hz, 1 H), 6.26 (d, J = 1.2 Hz, 1 H), 2.66 (s, 2 H), 1.37 (s, 6 H).

4.1.4. 7-((1-Hydroxy-1,3-dihydrobenzo[c] [1,2]oxaborol- 5-yl)oxy)-4H-chromen-4-one (29)

4.1.4.1. 2-nitro-5-((4-oxo-4H-chromen-7-yl)oxy)benzaldehyde(13). To a solution of 7-hydroxy-4*H*-chromen-4-one (7.54 g, 46.5 mmol, 1eq) in DMF (55 mL) were added 5-fluoro-2-nitrobenzaldehyde (8.65 g, 51.2 mmol, 1.1eq) and K_2CO_3 (9.64 g, 69.8 mmol, 1.5eq), and the reaction mixture was stirred for 1 h at 80 °C. The mixture was cooled to 0 °C, poured to 0.5 N HCl solution (165 mL) and stirred for 30 min at room temperature. Following filtration, the precipitate was washed with water (20 mL × 3) to afford intermediate **13** as a brown solid. Yield 96.7%; ^{1}H NMR (400 MHz, DMSO-d_6):δ10.26 (s, 1H), 8.30 (d, J = 6.0 Hz, 1H), 8.27 (d, J = 8.8 Hz, 1H), 8.13 (d, J = 8.8 Hz, 1H), 7.58–7.55 (m, 1H), 7.49–7.47 (m, 2H), 7.31–7.28(dd, J_1 = 1.6 Hz, J_2 = 8.8 Hz, 1H), 6.38 (d, J = 6.0 Hz, 1H).

4.1.4.2. 2-Amino-5-((4-oxo-4H-chromen-7-yl)oxy)benzaldehyde (17). To a solution of 2-nitro-5-((4-oxo-4*H*-chromen-7-yl)oxy) benzaldehyde (13.6 g, 43.7 mmol, 1eq) in MeOH(200 mL) and DCM(200 mL) was added Pd/C (10%, 1.36 g), and the reaction mixture was stirred for 24 h at room temperature under H_2 atmosphere (15 psi). The reaction mixture was filtered through Celite, and the filtrate was concentrated in vacuo. The residue was purified by column chromatography using EA/PE (1:10–1:3) as the eluent to give intermediate 8 as a yellow powder. Yield 39.8%; ^{1}H NMR (400 MHz, DMSO-d_6):δ9.82 (s, 1H), 8.23 (d, J = 6.0 Hz, 1H), 8.02 (d, J = 8.8 Hz, 1H), 7.47 (d, J = 2.8 Hz, 1H), 7.26–7.23 (m, 1H), 7.19 (s, 2H), 7.11–7.08(dd, J_1 = 2.4 Hz, J_2 = 6.4 Hz, 1H), 6.98 (d, J = 2.4 Hz, 1H), 6.89 (d, J = 9.2 Hz, 1H), 6.30 (d, J = 6.0 Hz, 1H).

4.1.4.3. 2-Bromo-5-((4-oxo-4H-chromen-7-yl)oxy)benzaldehyde (21). To a solution of 2-amino-5-((4-oxo-4*H*-chromen-7-yl)oxy) benzaldehyde (4.96 g, 17.7 mmol, 1eq) in anhydrous CH_3CN(40 mL) were added $CuBr_2$ (5.93 g, 26.6 mmol, 1.5eq) and t-BuONO (2.74 g, 26.6 mmol, 1.5eq) at −10 °C. The reaction mixture was stirred for 3 h at room temperature under N_2 atmosphere. The reaction mixture was filtered through Celite, and the filtrate was concentrated in vacuo. The residue was purified by column chromatography using DCM/EA/PE (1:1:10) as the eluent to give intermediate 9 as a white powder. Yield 55.9%; ^{1}H NMR (400 MHz, DMSO-d_6):δ10.19 (s, 1H), 8.28 (d, J = 6.0 Hz, 1H), 8.08 (d, J = 8.8 Hz, 1H), 7.90 (d, J = 8.4 Hz, 1H), 7.55 (d, J = 2.8 Hz, 1H), 7.50–7.48 (m, 1H), 7.28 (d, J = 2.0 Hz, 1H), 7.21–7.18(dd, J_1 = 2.0 Hz, J_2 = 8.8 Hz, 1H), 6.35 (d, J = 6.0 Hz, 1H).

4.1.4.4. 5-((4-oxo-4H-chromen-7-yl)oxy)-2-(4,4,5,5-tetramethyl-1,3,2-dioxaborolan -2-yl) benzaldehyde (25). To a solution of 2-bromo-5-((4-oxo-4*H*-chromen-7-yl)oxy)benzaldehyde (1.46 g,

4.23 mmol, 1eq) in 1, 4-dioxane (60 mL) were added bis(pinacolato) diboron (2.15 g, 8.46 mmol, 2eq), AcOK (1.25 g, 12.7 mmol, 3eq) and Pd (dppf)Cl_2 (0.16 g, 0.21 mmol, 0.05eq) at room temperature. After being stirred overnight at 60 °C under N_2 atmosphere, the reaction mixture was filtered through Celite. The filtrate was concentrated in vacuo, and the residue was purified by column chromatography using EA/PE (1:10–1:1) as the eluent to give the title intermediate as a yellow oil. Yield 96.3%.

4.1.4.5. 7-((1-Hydroxy-1,3-dihydrobenzo[c] [1,2]oxaborol-5-yl)oxy)-4H-chromen-4-one (29). To a solution of 5-((4-oxo-4*H*-chromen-7-yl)oxy)-2-(4,4,5,5-tetramethyl-1,3,2- dioxaborolan-2-yl) benzaldehyde (1.60 g, 4.08 mmol, 1eq) in MeOH(4 mL) was added $NaBH_4$ (0.23 g, 6.12 mmol, 1.5eq) in portions at 0 °C. After being stirred for 30 min at room temperature, the reaction mixture was cooled to 0 °C and quenched with water (1 mL). The pH was then adjusted to 3 with HCl solution (6 N), and the resultant mixture was stirred for 30 min. Following filtration, the precipitate was washed with water (2 mL × 3) and further purified by prep-TLC (PE/DCM = 1:2) to give 7-((1-hydroxy-1,3-dihydrobenzo [c] [1,2] oxaborol-5-yl)oxy)-4H-chromen-4-one as a white solid. Yield 16.7%; ^{1}H NMR (400 MHz, DMSO-d_6): δ ppm 9.19 (s, 1 H), 8.21 (d, J = 6.0 Hz, 1 H), 8.01–8.03 (m, 1 H), 7.78 (d, J = 7.6 Hz, 1 H), 7.17 (br, 1 H), 7.12 (br, 2 H), 7.10 (t, J = 2.4 Hz, 1 H), 6.29 (d, J = 6.0 Hz, 1 H), 4.95 (s, 2 H), ^{13}C NMR (100 MHz, DMSO-d_6) δ: 176.10, 161.77, 157.78, 157.31, 133.08, 132.66, 127.78, 120.49, 119.54, 119.39, 116.83, 113.15, 112.79, 61.61, 70.17. ESI-HRMS: m/z calcd for $C_{16}H_{11}BO_5$ $[M+H]^+$ 295.0778, found 295.0780.

Compounds **30**–**32** were prepared via a similar procedure to that for **29**, and the data for structural characterization of the intermediates and target compounds were provided in the supporting information.

4.1.5. Methyl 5-((1-hydroxy-1, 3-dihydrobenzo[c] [1,2]oxaborol-5-yl)oxy)pyrazolo [1,5-a] pyrimidine-3-carboxylate (63)

4.1.5.1. 5-Hydroxy-2-(4,4,5,5-tetramethyl-1,3,2-dioxaborolan-2-yl) benzaldehyde (43). To a solution of 2-bromo-5-hydroxybenzaldehyde (2.0 g, 9.95 mmol, 1eq) in 1,4-dioxane(45 mL) were added bis(pinacolato)diboron (3.16 g, 12.44 mmol, 1.25eq), AcOK (2.93 g, 29.8 mmol, 3eq) and Pd (dppf) Cl_2 (364 mg, 0.49 mmol, 0.05eq) at room temperature. After being stirred for 1 h at 100 °C under N_2 atmosphere, the reaction mixture was cooled to room temperature and filtered through on Celite. The filtrate was concentrated in vacuo and the residue was purified by column chromatography using EA/PE (1:10) as the eluent to give the title intermediate as a pale yellow solid. Yield 87.9%.

4.1.5.2. Methyl 5-(3-formyl-4-(4,4,5,5-tetramethyl-1,3,2-dioxaborolan-2-yl) phenoxy) pyrazolo [1,5-a] pyrimidine-3-carboxylate (53). To a solution of 5-hydroxy-2-(4,4,5,5-tetramethyl-1,3,2-dioxaborolan-2-yl) benzaldehyde (2.15 g, 8.67 mmol, 1eq) in MeOH(20 mL) was added $NaBH_4$ (426 mg, 11.3 mmol, 1.3eq) in portions. The reaction mixture was stirred for 30 min at room temperature. Afterwards, the pH of the mixture was adjusted to 2 with HCl solution (3 N), and the resultant mixture was stirred overnight at room temperature. The mixture was concentrated in vacuo, and the precipitate was filtered and washed with water (3 mL × 3) to afford intermediate as a white solid. Yield 57.7%.

4.1.5.3. Methyl 5-((1-hydroxy-1,3-dihydrobenzo[c] [1,2]oxaborol-5-yl)oxy)pyrazolo [1,5-a] pyrimidine -3-carboxylate (63). To a solution of benzo [*c*] [1,2]oxaborole-1,5(3*H*)-diol (35 mg, 0.24 mmol, 1eq) in DMF(2 mL) were added methyl 5-chloropyrazolo [1,5-*a*] pyrimidine -3-carboxylate (50 mg, 0.24 mmol, 1eq) and Cs_2CO_3 (154 mg, 0.47 mmol, 2eq), and the reaction mixture was stirred for 30 min at 50 °C. Afterwards, the mixture was cooled to room temperature, and the pH was adjusted to 2 with HCl solution (3 N). Following filtration, the precipitate was washed with water (3 mL × 3) to afford the title compound as a white solid. Yield 58.6%.^{1}H NMR (400 MHz, DMSO-d_6): δppm 9.26 (s, 1 H), 9.20 (d, J = 7.28 Hz, 1 H), 8.48 (s, 1 H), 7.83 (d, J = 8.03 Hz, 1 H), 7.44 (s, 1 H), 7.32 (d, J = 7.78 Hz, 1 H), 6.98 (d, J = 7.53 Hz, 1 H), 5.03 (s, 2 H), 3.67 (s, 3 H); ^{13}C NMR (100 MHz, DMSO-d_6) δ 163.36, 162.25, 156.29, 154.88, 147.61, 146.65, 140.71, 132.26, 121.07, 114.92, 102.11, 100.85, 70.20, 51.33. ESI-HRMS: m/z calcd for $C_{15}H_{12}BN_3O_5$ $[M+H]^+$ 326.0948, found 326.0949.

Compounds **64**–**72** were prepared via a similar procedure to that for **63**, and the data for structural characterization of the intermediates and target compounds were provided in the supporting information.

4.2. Biological evaluation

4.2.1. PDE biochemical assay

The inhibitory activity against PDEs was tested by measuring the hydrolysis of [^{3}H]-cAMP or [^{3}H]-cGMP into [^{3}H]-AMP or [^{3}H]-GMP, respectively, using a phosphodiesterase scintillation proximity assay (SPA). The protein was diluted to a concentration of 1–2 nM with an assay buffer (50 mM Tris pH 7.5, 8.3 mM $MgCl_2$, 1.7 mM EGTA). For PDE1A, PDE1B, PDE1C, the reaction buffer also contained 0.2 mM $CaCl_2$ and 0.36 mM calmodulin. The compound solution experienced 3-fold serial dilution for 10 doses, and Crisaborole was introduced as the reference compound. The reaction assay was initiated by successively adding 80 μL of protein solution, 10 μL of test compound solution, and 10 μL of [^{3}H]-cAMP or [^{3}H]-cGMP (0.5 μCi/mL) to a "low binding" plate, and all reactions were carried out in duplicate. The plate was incubated at 30 °C for 30 min, and the reaction was terminated by addition of phosphodiesterase SPA beads (50 μL, RPNQ0150, PerkinElmer Inc.). All plates were settled for 20 min before being counted with a MicroBeta 2 (PerkinElmer Inc.) counter. All experimental data were analyzed by using GraphPad Prism 5.0 to determine IC_{50} values.

4.2.2. Assay for evaluating the effect on PMA-induced mouse ear oedema

The ethanolic extract containing target compounds were topically administrated (1.0 mg/ear in ethanol) before PMA application, and the positive reference group was treated with Crisaborole (1 mg/ear in acetone). The right ear of ICR mice (male, 8-week-old) received PMA (2 μg/ear, in 20 μL acetone) to induce oedema, while the left ear, as the blank, received acetone (20 μL). After 4 h, the animals were euthanized by cervical dislocation, and thickness of both ears were measured by micrometer. Ear oedema was determined as the difference between the thickness of both ears. The inhibition percentage was expressed as a reduction in thickness compared to the model group.

4.2.3. Assay for evaluating the efficacy against calcipotriol-induced AD in mice

According to a published protocol, the low-calcemic analogue of vitamin D3, calcipotriol (purchased from Sigma, 2 nM, 20 μL, dissolved in ethanol), was applied topically to the dorsal side of left ear for establishing AD mouse model [34]. A total of 32 mice were randomly assigned into four groups: normal group, AD model group, the group treated by the ointment of Crisaborole, and the group treated by the ointment of **72**. The ointment of Crisaborole and the ointment of **72** were administered to the dorsal side of left ear twice a day (30 mg/kg) for 14 days, while normal group received ethanol (20 μL). At the 17th day, the animals were anaesthetized with 10% chloral hydrate. A micrometer (Oditest Kroeplin) was used for measuring ear thickness, and the obvious increase in ear

thickness, calculated by subtracting the thickness of the left ear (vehicle) from the thickness of the right ear (calcipotriol-treated), indicated that the ear was oedematous. Upon comparing the treated and non-treated animals, the percentage of inhibition of the inflammatory reaction was determined.

4.3. Toxicity

4.3.1. Repeated dose toxicity

Healthy male and female Sprague-Dawley rats (8-week old) were randomly divided into three groups with each group containing 6 male animals and 6 female ones. 1% CMC-Na (for vehicle group) or graded doses of compound **72** (400 and 700 mg/kg) were administered to corresponding group by oral gavage once daily for 14 days. The rats were observed daily for mortality and clinical signs, and body weights were recorded on day 0, 7 and 14. Finally, all rats were euthanized by isoflurane (2%–5%) inhalation, and their organs were then collected for macroscopic necropsy examination. The weights of liver, kidney, testis, thymus, heart and lung were measured.

4.3.2. Skin phototoxicity test

30 healthy albino guinea pigs (250–300 g) were randomly divided into 5 groups, including 8-MOP-treated group, **72** (5 mg/kg, 10 mg/kg, 24 mg/kg)-treated groups, and Crisaborole (10 mg/kg)-treated group. Four 2 cm × 2 cm skin-cleared hair removal areas were prepared on both sides of the animal's spine 24 h before the experiment, and 0.2 mL of the tested substances were applied to the hair removal areas. Afterwards, the animals were placed into restrainers and exposed to UVA light for 40 min. The average light intensity of 6.0 cm from the back area of the tested objects was 4.2 mw/cm^2 measured by a radiation meter. After light exposure, the animals were euthanized by atipamezole (0.06 mg/kg) upon intraperitoneal injection. Irradiated skin areas were observed macroscopically at 1, 24, 48, and 72 h after the end of the light irradiation for erythema, eschar, oedema and its degree.

At 72 h after light irradiation, the time course of skin lesions was investigated. To thick paper, skin samples were attached in a flat orientation using a stapler, and they were then fixed with neutral buffered formalin (10 vol%), embedded in paraffin, sectioned, stained with hematoxylin and eosin (HE), and examined microscopically by a certified pathologist. To ensure the quality of the pathology data, the results were reviewed by a second certified pathologist.

4.4. Molecular docking

The molecular docking analysis was performed utilizing C-DOCKER module of Discovery Studio 2017r2 (Accelrys Software, Inc., San Diego, CA, USA). The co-crystal structure of AN2898 bound to PDE4B was obtained from Protein Data Bank. The OPLS-2005-force field was applied to the protein after the removal of original ligand and solvent molecules from the co-crystal structure. 3D structure of the ligand was generated, and the energy minimization performed. The ligand was then docked into the active site of the receptor, which was defined according to the location of AN2898 in the enzyme. The calculated C-DOCKING ENERGE was employed for determining the ultimate binding conformation. The graphical representation was generated using PyMOL.

Declaration of competing interest

The authors declare that they have no known competing financial interests or personal relationships that could have appeared to influence the work reported in this paper.

Acknowledgment

This work was supported by National Major Scientific and Technological Special Project for "Significant New Drugs Development" (2012ZX09401006), the Outstanding Scientific and Technological Innovation Team Projects of Jiangsu Province, China (2015).

Appendix A. Supplementary data

Supplementary data to this article can be found online at https://doi.org/10.1016/j.ejmech.2021.113171.

References

[1] H. Williams, C. Robertson, A. Stewart, N. Aït-Khaled, G. Anabwani, R. Anderson, I. Asher, R. Beasley, B. Björkstén, M. Burr, T. Clayton, J. Crane, P. Ellwood, U. Keil, C. Lai, J. Mallol, F. Martinez, E. Mitchell, S. Montefort, N. Pearce, J. Shah, B. Sibbald, D. Strachan, E. von Mutius, S.K. Weiland, Worldwide variations in the prevalence of symptoms of atopic eczema in the international study of asthma and allergies in childhood, J. Allergy Clin. Immunol. 103 (1 Pt 1) (1999) 125–138.
[2] K. Malik, K.D. Heitmiller, T. Czarnowicki, An update on the pathophysiology of atopic dermatitis, Dermatol. Clin. 35 (3) (2017) 317–326.
[3] W. David Boothe, J.A. Tarbox, M.B. Tarbox, Atopic dermatitis: pathophysiology, Adv. Exp. Med. Biol. 1027 (2017) 21–37.
[4] J.N. Mayba, M.J. Gooderham, Review of atopic dermatitis and topical therapies, J. Cutan. Med. Surg. 21 (3) (2017) 227–236.
[5] S. Amar, R. Gilhen, Z. Jorge, Al A. Fadi, P. Anupam, High-dose caspofungin as a component of combination antifungal therapy in 91 patients with neoplastic diseases and hematopoietic stem cell transplantation: a critical review of short-term and long-term adverse events, J. Pharm. Pract. 28 (2) (2015) 171–182.
[6] T. Dainichi, A. Kitoh, A. Otsuka, S. Nakajima, T. Nomura, D.H. Kaplan, K. Kabashima, The epithelial immune microenvironment (EIME) in atopic dermatitis and psoriasis, Nat. Immunol. 19 (12) (2018) 1286–1298.
[7] T. Gavrilova, Immune dysregulation in the pathogenesis of atopic dermatitis, Dermatitis 29 (2) (2018) 57–62.
[8] N.K. Tulsian, S. Krishnamurthy, G.S. Anand, Channeling of cAMP in PDE-PKA complexes promotes signal adaptation, Biophys. J. 112 (12) (2017) 2552–2566.
[9] M.G. Beltejar, H.T. Lau, M.G. Golkowski, S.E. Ong, J.A. Beavo, Analyses of PDE-regulated phosphoproteomes reveal unique and specific cAMP-signaling modules in T cells, Proc. Natl. Acad. Sci. U.S.A. 114 (30) (2017) E6240–E6249.
[10] I.S. Lazaros, M. Athanasios, P.B. Dimitrios, Phosphodiesterase 4 inhibitors in immune-mediated diseases: mode of action, clinical applications, current and future perspectives, Curr. Med. Chem. 24 (28) (2017) 3054–3067.
[11] P. Ting, G. Jun, J. Yongzhe, Z. Yanping, T. Rongsheng, W. Xin, B. Lan, S. Jianyou, Inhibitors of phosphodiesterase as cancer therapeutics, Eur. J. Med. Chem. 150 (2018) 742–756.
[12] T.E. Woo, P. Kuzel, Crisaborole 2% ointment (eucrisa) for atopic dermatitis, Skin Therapy Lett 24 (2) (2019) 4–6.
[13] L.T. Zane, L. Kircik, R. Call, E. Tschen, Z.D. Draelos, S. Chanda, M. Van Syoc, A.A. Hebert, Crisaborole topical ointment, 2% in patients ages 2 to 17 years with atopic dermatitis: a phase 1b, open-label, maximal-use systemic exposure study, Pediatr. Dermatol. 33 (4) (2016) 330–337.
[14] L.T. Zane, S. Chanda, K. Jarnagin, D.B. Nelson, L. Spelman, L.S. Gold, Crisaborole and its potential role in treating atopic dermatitis: overview of early clinical studies, Immunotherapy 8 (8) (2016) 853–866.
[15] Y.R. Freund, T. Akama, M.R. Alley, J. Antunes, C. Dong, K. Jarnagin, R. Kimura, J.A. Nieman, K.R. Maples, J.J. Plattner, F. Rock, R. Sharma, R. Singh, V. Sanders, Y. Zhou, Boron-based phosphodiesterase inhibitors show novel binding of boron to PDE4 bimetal center, FEBS Lett. 586 (19) (2012) 3410–3414.
[16] Y. Donglei, B. Arnold, K. Nicole, W. Carl, A. Graham, L. Kuo-Hsiung, anti-HIV Agents. Part 55. 3′R, 4′R-Di-(O)-(-)-camphanoyl-2′,2′-dimethyldihydropyrano [2,3-f]chromone (DCP), a Novel anti-HIV Agent, ChemInform 34 (32) (2003) 1575–1576.
[17] Richard Y. Huang, Patrick T. Franke, Norman Nicolaus, Mark Lautens Domino CeH functionalization reactions of gem-dibromoolefins: synthesis of N-fused benzo[c]carbazoles, Tetrahedron 69 (2013) 4395–4402.
[18] Y.L. Su, B.W. Xiao, S.X. Sai, J. Neng, D.G.W. Kelvin, Q.Y. He, B.S. Hong, Y.K. Ling, Multifunctional tacrine flavonoid hybrids with cholinergic, b-amyloid-reducing, and metal chelating properties for the treatment of Alzheimer's disease, Eur. J. Med. Chem. 69 (2013) 632–646.
[19] M. Matveenko, O.J. Kokas, M.G. Banwell, C.W. Anthony, Chemoenzymatic approaches to lycorine-type Amaryllidaceae alkaloids: total syntheses of ent-lycoricidine, 3-epi-ent-Lycoricidine, and 4-Deoxy-3-epient -lycoricidine, Org. Lett. 9 (18) (2007) 3683–3685.
[20] C. John, J. Christoph, Fahrni Fluorescence sensing based on cation-induced conformational switching: copper-selective modulation of the photoinduced intramolecular charge transfer of a donor–acceptor biphenyl fluorophore,

Tetrahedron 60 (2004) 11099–11107.
[21] W. Shi-Hui, W. Yan, Z. Yu-Ying, H. Jian, Z. Yi-Fan, K. Diwa, L. Da-Wei, H. Chun, Synthesis, characterization, crystal structure and cytotoxicities of 2-aroyl-3-aryl-5H-furo[3,2-g] chromene derivatives, ARKIVOC 11 (2010) 204–214.
[22] P.G. Tsoungas, M. Searcey, A convenient access to benzo-substituted phthalazines as potential precursors to DNA intercalators, Tetrahedron Lett. 42 (37) (2001) 6589–6592.
[23] D. Pajtás, K. Dihen, K. Kónya, L. Peter, Regioselective suzuki-miyaura reactions of the bis(triflate) of 6,7-Dihydroxy-2,2-dimethyl- chroman-4-one, Synlett 27 (07) (2016) 1073–1076, https://doi.org/10.1055/s-0035-1561265.
[24] T. Tibor, J. J Csaba, A novel synthesis of precocenes. Efficient synthesis and regioselective O-alkylation of dihydroxy-2,2-dimethyl-4- chromanones, J. Heterocycl. Chem. 25 (3) (1988) 871–877.
[25] S.L. Byoung, H.L. Jae, Y.C. Dae, Novel synthesis of 2-chloroquinolines from 2-vinylanilines in nitrile solvent, J. Org. Chem. 67 (2002) 7884–7886.
[26] F. Zaragoza, H. Stephensen, B. Peschke, Karin Rimvall, 2-(4-Alkylpiperazin-1-yl) quinolines as a New class of imidazole-free histamine H3 receptor antagonists, J. Med. Chem. 48 (1) (2005) 306–311.
[27] B. Zhou, C. Jiang, V.R. Gandi, Y. Lu, T. Hayashi, Palladium-catalyzed asymmetric arylation of trifluoromethylated/perfluoroalkylated 2-quinazolinones with high enantioselectivity, Chemistry 22 (37) (2016) 13068–13071.
[28] K. Naidoo, F. Jagot, L. van den Elsen, C. Pellefigues, A. Jones, H. Luo, K. Johnston, G. Painter, B. Roediger, J. Lee, W. Weninger, G. Le Gros, E. Forbes-Blom, Eosinophils determine dermal thickening and water loss in a MC903 model of atopic dermatitis, J. Invest. Dermatol. 38 (12) (2018) 2606–2616.
[29] V. Moosbruggermartinz, M. Schmuth, S. Dubrac, A mouse model for atopic dermatitis using topical application of vitamin D3 or of its analog MC903, Methods Mol. Biol. 1559 (2017), 91-72.
[30] J. Choi, J.R. Kim, H. Kim, Y.A. Kim, H.J. Lee, J. Kim, K.W. Lee, The atopic dermatitis-like symptoms induced by MC903 were alleviated in JNK1 knockout mice, Toxicol. Sci. 136 (2) (2013) 443–449.
[31] D.D. Hou, W. Zhang, Y.L. Gao, Y.Z. Sun, H.X. Wang, R.Q. Qi, H.D. Chen, X.H. Gao, Anti-inflammatory effects of quercetin in a mouse model of MC903-induced atopic dermatitis, Int. Immunopharm. 74 (2019) 105676.
[32] K. Kazuhiro, Y. Hironobu, S. Yumi, H. Yumiko, S. Fumi, M. Yumiko, T. Yuki, M. Makoto, S. Keiichiro, The abdominal skin of female Sprague-Dawley rats is more sensitive than the back skin to drug-induced phototoxicity, J. Pharmacol. Toxicol. Methods (2017) 46–55.
[33] Y.X. Yi, A. Gaurav, G.A. Akowuah, Docking studies of curcumin and analogues with various phosphodiesterase 4 subtypes, Curr. Drug Discov. Technol. 17 (2) (2020) 248–260.
[34] X.J. Liu, Z.L. Mu, Y. Zhao, J.Z. Zhang, Topical tetracycline improves MC903-induced atopic dermatitis in mice through inhibition of inflammatory cytokines and thymic stromal lymphopoietin expression, Chin. Med. J. 129 (12) (2016) 1483–1490.